Communications in Theoretical Physics

Commun. Theor. Phys. **77** (2025) 065403 (12pp) https://doi.org/10.1088/1572-9494/ad9c3e
CSTR: 32041.14.CTP.ad9c3e

Prospects for searching for sterile neutrinos with gravitational wave and γ-ray burst joint observations

Lu Feng[1,2,5], Tao Han[2,5], Jing-Fei Zhang[2] and Xin Zhang[2,3,4,*]

[1] College of Physical Science and Technology, Shenyang Normal University, Shenyang 110034, China
[2] Liaoning Key Laboratory of Cosmology and Astrophysics, College of Sciences, Northeastern University, Shenyang 110819, China
[3] MOE Key Laboratory of Data Analytics and Optimization for Smart Industry, Northeastern University, Shenyang 110819, China
[4] National Frontiers Science Center for Industrial Intelligence and Systems Optimization, Northeastern University, Shenyang 110819, China

E-mail: zhangxin@mail.neu.edu.cn

Received 5 September 2024, revised 20 November 2024
Accepted for publication 26 November 2024
Published 27 February 2025

Abstract

Sterile neutrinos can influence the evolution of the Universe, and thus cosmological observations can be used to detect them. Future gravitational-wave (GW) observations can precisely measure absolute cosmological distances, helping to break parameter degeneracies generated by traditional cosmological observations. This advancement can lead to much tighter constraints on sterile neutrino parameters. This work provides a preliminary forecast for detecting sterile neutrinos using third-generation GW detectors in combination with future short γ-ray burst observations from a THESEUS-like telescope, an approach not previously explored in the literature. Both massless and massive sterile neutrinos are considered within the ΛCDM cosmology. We find that using GW data can greatly enhance the detection capability for massless sterile neutrinos, reaching 3σ level. For massive sterile neutrinos, GW data can also greatly assist in improving the parameter constraints, but it seems that effective detection is still not feasible.

Keywords: sterile neutrino, gravitational wave, standard siren, short gamma-ray burst, cosmological observation

1. Introduction

On August 17$^{\text{th}}$ 2017, the first observation of gravitational waves (GW) from a binary neutron star (BNS) merger [1], together with the first joint observation of GW from a BNS merger and its electromagnetic (EM) counterpart [2, 3], marked the beginning of a new era in multi-messenger astronomy and cosmology. The measurement of the GW signal directly provides information on the absolute luminosity distance to the source, while its redshift can be determined by identifying the EM counterpart of the GW source. This establishes an absolute distance-redshift relation, known as the standard siren method, which is crucial for cosmological studies. To date, only one bright siren, GW170817, has been identified. This is insufficient to probe cosmological parameters using current standard sirens, necessitating the use of next-generation GW detectors.

In the future, third-generation (3G) ground-based GW detectors, such as the Einstein Telescope (ET) [4, 5] in Europe and the Cosmic Explorer (CE) [6, 7] in the United States will become operational, with sensitivities improved one order of magnitude over the current detectors, and much more BNS merger events will be observed at much deeper redshifts. Recently, GW standard sirens have been widely discussed in the literature [8–47]. It has been found that future observations of GW standard sirens from the ET and CE will

[5] These authors contributed equally to this paper.
[*] Author to whom any correspondence should be addressed.

play a crucial role in the estimation of cosmological parameters [14, 16, 22, 25, 26, 28, 37, 38, 43, 46]. In particular, the GW standard sirens can break the parameter degeneracies generated by the current EM cosmological observations, thereby improving constraints on neutrino mass, see [14, 37].

A recent forecast [46] demonstrated that joint observations of BNS by 3G GW detectors and short γ-ray burst (GRB) observations by missions similar to the THESEUS satellite project can improve the constraints on the total active neutrino mass. Therefore, it is crucial to investigate how the combined GW-GRB observations would affect constraints on the sterile neutrino parameters.

The existence of light sterile neutrinos has been suggested by anomalies in short-baseline (SBL) neutrino experiments [48–57]. To explain the SBL neutrino oscillation data, sterile neutrinos with eV-scale masses are required [58–60]. Cosmological observations play a crucial role in constraining the mass of active neutrinos (see [61–108]). Since sterile neutrinos have implications for the evolution of the Universe, cosmology can provide an independent test for their existence. For related works on sterile neutrinos, see [109–134].

Currently, one of the most significant challenges in cosmology is the 'Hubble tension' [135], which refers to the discrepancy between early and late Universe observations. In the past few years, people often considered models that include light sterile neutrinos to alleviate the Hubble constant crisis. This is because when using the cosmic microwave background data to constrain cosmological parameters, the effective number of neutrino species ($N_{\rm eff}$) is positively correlated with the Hubble constant; if $N_{\rm eff}$ is larger, the derived Hubble constant will also be larger. See [118, 125–128, 130, 131, 134], for related studies. However, in recent years, the results of cosmological observation fits have shown that the effect of using this method to alleviate the Hubble crisis is no longer significant. Nevertheless, due to the significant correlation between $N_{\rm eff}$ and H_0, precise measurements of the Hubble constant using gravitational wave standard sirens are very helpful for determining the parameters of sterile neutrinos.

Additionally, the main advantage of the standard siren method for measuring the Hubble constant is that it avoids relying on the cosmic distance ladder. Therefore, in the future, the GW standard sirens could become a promising cosmological probe, playing a crucial role in measuring cosmological parameters, including those related to sterile neutrinos.

In this paper, we present a forecast for the search for sterile neutrinos using joint GW-GRB observations. The primary aim of this work is to investigate the impact of future GW standard siren observations on the constraints of sterile neutrino parameters.

This work is organized as follows. In section 2, we introduce the methodology used in this work. In section 3, we give the constraint results and make some relevant discussions. The conclusion is given in section 4.

2. Methodology

2.1. Gravitational wave simulation

In this subsection, we introduce the method of simulating the joint GW standard sirens and GRB events. We consider the THESEUS-like GRB detector in synergy with the 3G GW observation. We use the simulation method as prescribed in [43, 46]. Here, we provide only a brief overview.

The BNS merger rate with redshift in the observer frame is [136–138]

$$R_{\rm m}(z) = \frac{\mathcal{R}_{\rm m}(z)}{1+z}\frac{{\rm d}V(z)}{{\rm d}z}, \tag{1}$$

where ${\rm d}V(z)/{\rm d}z$ is the comoving volume element, the factor $(1+z)^{-1}$ converts the merger rate in the source frame to the observer frame, and $\mathcal{R}_{\rm m}(z)$ is the BNS merger rate in the source frame, expressed as

$$\mathcal{R}_{\rm m}(z) = \int_{t_{\rm min}}^{t_{\rm max}} \mathcal{R}_{\rm f}[t(z) - t_{\rm d}]P(t_{\rm d}){\rm d}t_{\rm d}, \tag{2}$$

which is commonly used in the literature [137–147][6]. Here, $t_{\rm d}$ is the delay time between the formation of BNS system and merger, $t_{\rm min} = 20$ Myr is the minimum delay time, $t_{\rm max} = t_{\rm H}$ is the maximum delay time, $t(z)$ is the age of the Universe at the time of merger, $\mathcal{R}_{\rm f}$ is the cosmic star formation rate in the source frame for which we adopt the Madau–Dickinson model [149], $P(t_{\rm d})$ is the time delay distribution of the $t_{\rm d}$, and we adopt the exponential time delay model [136], which is given by

$$P(t_{\rm d}) = \frac{1}{\tau}\exp(-t_{\rm d}/\tau), \tag{3}$$

with an e-fold time of $\tau = 0.1$ Gyr for $t_{\rm d} > t_{\rm min}$.

In our calculations, for BNS mergers, we consider the local comoving merger rate to be $\mathcal{R}_{\rm m}(z=0) = 920 \quad {\rm Gpc}^{-3}\ {\rm yr}^{-1}$, which is the estimated median from the O1 LIGO and the O2 LIGO/Virgo observation run [150] and is also consistent with the O3 observation run [151]. We simulate a catalog of BNS mergers for 10 years observation. For each source, the location (θ, ϕ), the polarization angle ψ, the cosine of the inclination angle ι, and the coalescence phase $\psi_{\rm c}$ are drawn from uniform distributions. Currently, there are multiple candidate models for the neutron star (NS) mass distribution. However, different mass distributions of NSs have less impact on the cosmological analysis [43]. For simplicity, we employ a Gaussian mass distribution. This distribution has a mean of $1.33M_\odot$ for the NS mass and a standard deviation of $0.09M_\odot$, where $M_\odot$ represents the solar mass [152, 153].

Under the stationary phase approximation [154], the Fourier transform of the frequency-domain GW waveform for a detector network (with N detectors) is given by [155, 156]

$$\tilde{\boldsymbol{h}}(f) = {\rm e}^{-{\rm i}\boldsymbol{\Phi}}\boldsymbol{h}(f), \tag{4}$$

[6] Here, we take into account the time dilation factor $(1+z)^{-1}$ in equation (1), which differs from the expression presented in [148]. In this paper, we adopt the commonly used formula in the literature, which is somewhat different from that given in [148].

with the $\boldsymbol{h}(f)$ is given by

$$\boldsymbol{h}(f) = \left[\frac{h_1(f)}{\sqrt{S_{\mathrm{n},1}(f)}}, \frac{h_2(f)}{\sqrt{S_{\mathrm{n},2}(f)}}, \ldots, \frac{h_N(f)}{\sqrt{S_{\mathrm{n},N}(f)}}\right]^{\mathrm{T}}, \tag{5}$$

where $\boldsymbol{\Phi}$ is the $N \times N$ diagonal matrix with $\Phi_{ij} = 2\pi f \delta_{ij}(\boldsymbol{n}\cdot\boldsymbol{r}_k)$, $\boldsymbol{n}$ is the propagation direction of GW, and $\boldsymbol{r}_k$ is the location of the k-th detector. Here $S_{\mathrm{n},k}(f)$ is the one-side noise power spectral density of the k-th detector, The Fourier transform of the GW waveform of k-th detector is given by

$$h_k(f) = \mathcal{A}_k f^{-7/6} \exp\{\mathrm{i}[2\pi f t_{\mathrm{c}} - \pi/4 - 2\psi_c + 2\Psi(f/2)] - \varphi_{k,(2,0)})\}, \tag{6}$$

where the Fourier amplitude can be written as

$$\mathcal{A}_k = \frac{1}{d_{\mathrm{L}}}\sqrt{(F_{+,k}(1+\cos^2\iota))^2 + (2F_{\times,k}\cos\iota)^2} \times \sqrt{5\pi/96}\,\pi^{-7/6}\mathcal{M}_{\mathrm{chirp}}^{5/6}. \tag{7}$$

Here, the detailed forms of $\Psi(f/2)$ and $\varphi_{k,(2,0)}$ can be found in [155, 157], d_{L} is the luminosity distance of the GW source, $\mathcal{M}_{\mathrm{chirp}} = (1+z)\eta^{3/5}M$ is the observed chirp mass, $\eta = m_1 m_2/M^2$ is the symmetric mass ratio, and $M = m_1 + m_2$ is the total mass of the binary system with component masses m_1 and m_2, $F_{+,k}$ and $F_{\times,k}$ are the antenna response functions of the k-th GW detector, we adopt the GW waveform in the frequency-domain, in which the time t is replaced by $t_{\mathrm{f}} = t_{\mathrm{c}} - (5/256)\mathcal{M}_{\mathrm{chirp}}^{-5/3}(\pi f)^{-8/3}$ [155, 157], where t_{c} is the coalescence time.

In this work, we consider the waveform in the inspiralling stage for the non-spinning BNS system. Here we adopt the restricted Post-Newtonian approximation and calculate the waveform to the 3.5 PN order [157, 158].

After simulating the GW catalog, we need to calculate the signal-to-noise ratio (SNR) for each GW event. The SNR for the detection network of N independent interferometers can be calculated by

$$\rho = (\tilde{\boldsymbol{h}}|\tilde{\boldsymbol{h}})^{1/2}. \tag{8}$$

The inner product is defined as

$$(\boldsymbol{a}|\boldsymbol{b}) = 2\int_{f_{\mathrm{lower}}}^{f_{\mathrm{upper}}} \{\boldsymbol{a}(f)\boldsymbol{b}^*(f) + \boldsymbol{a}^*(f)\boldsymbol{b}(f)\}\,\mathrm{d}f, \tag{9}$$

where * represents conjugate transpose, $\boldsymbol{a}$ and $\boldsymbol{b}$ are column matrices of the same dimension, the lower cutoff frequency is set to $f_{\mathrm{lower}} = 1$ Hz for ET and $f_{\mathrm{lower}} = 5$ Hz for CE, and $f_{\mathrm{upper}} = 2/(6^{3/2}2\pi M_{\mathrm{obs}})$ is the frequency at the last stable orbit with $M_{\mathrm{obs}} = (m_1 + m_2)(1+z)$. In this work, we adopt the SNR threshold to be 12 in our simulation.

For the short GRB model, we adopt the model of Gaussian structured jet profile based on the GW170817/GRB170817A [159] observation,

$$L_{\mathrm{iso}}(\theta_{\mathrm{v}}) = L_{\mathrm{on}}\exp\left(-\frac{\theta_{\mathrm{v}}^2}{2\theta_{\mathrm{c}}^2}\right), \tag{10}$$

where θ_{v} is the viewing angle, $L_{\mathrm{iso}}(\theta_{\mathrm{v}})$ is the isotropically equivalent luminosity of short GRB observed at different θ_{v}, $L_{\mathrm{on}} = L_{\mathrm{iso}}(0)$ is the on-axis isotropic luminosity, $\theta_{\mathrm{c}} = 4.7^\circ$ is the characteristic angle of the core, and the direction of the jet is assumed to align with the binary orbital angular momentum, namely $\iota = \theta_{\mathrm{v}}$.

For the distribution of the short GRB, we assume the empirical broken-power-law luminosity function[7]

$$\Phi(L) \propto \begin{cases}(L/L_*)^{\alpha}, & L < L_*,\\ (L/L_*)^{\beta}, & L \geqslant L_*,\end{cases} \tag{11}$$

which is commonly used in the literature [38, 42, 43, 46, 137, 138, 146, 148]. Here, L is the isotropic rest frame luminosity in the $1-10000$ keV energy range, L_* is the characteristic luminosity that separates the low and high end of the luminosity function, and the slopes describing these regimes are given by α and β, respectively. Following [146], we adopt $L_* = 2\times10^{52}$ erg sec^{-1}, $\alpha = -1.95$, and $\beta = -3$. We assume a standard low end cutoff in luminosity of $L_{\mathrm{min}} = 10^{49}$ erg sec^{-1}, and we also term the on-axis isotropic luminosity L_{on} as the peak luminosity L [43, 137, 138, 160]. For the THESEUS mission [161], a GRB detection is recorded if the value of observed flux is greater than the flux threshold $P_{\mathrm{T}} = 0.2\mathrm{p}hs^{-1}\mathrm{cm}^{-2}$ in the 50-300 keV band. For the GRB detection, we assume a duty cycle of 80% and a sky coverage fraction of 0.5. From the GW catalogue which has passed the threshold 12, we can select the GW-GRB events according to the probability distribution $\Phi(L)\mathrm{d}L$.

For a network with N independent interferometers, the Fisher information matrix is given by

$$F_{ij} = \left(\frac{\partial\tilde{\boldsymbol{h}}}{\partial\theta_i}\middle|\frac{\partial\tilde{\boldsymbol{h}}}{\partial\theta_j}\right), \tag{12}$$

where θ_i denotes nine GW parameters (d_{L}, $\mathcal{M}_{\mathrm{chirp}}$, η, θ, ϕ, ι, t_{c}, ψ_{c}, ψ) for a GW event.

For the total uncertainty of the luminosity distance d_{L}, we first consider the instrumental error $\sigma_{d_{\mathrm{L}}}^{\mathrm{inst}}$. The covariance matrix is equal to the inverse of the Fisher information matrix, thus the instrumental error of GW parameter θ_i is

$$\Delta\theta_i = \sqrt{(F^{-1})_{ii}}, \tag{13}$$

where F_{ij} is the total Fisher information matrix for the network of N interferometers.

In addition, the weak-lensing error $\sigma_{d_{\mathrm{L}}}^{\mathrm{lens}}$ and the peculiar velocity error $\sigma_{d_{\mathrm{L}}}^{\mathrm{pv}}$ are also considered. The error caused by weak lensing is adopted from [162, 163],

$$\sigma_{d_{\mathrm{L}}}^{\mathrm{lens}}(z) = \left[1 - \frac{0.3}{\pi/2}\arctan(z/0.073)\right]\times d_{\mathrm{L}}(z) \times 0.066\left[\frac{1-(1+z)^{-0.25}}{0.25}\right]^{1.8}. \tag{14}$$

For the error caused by the peculiar velocity of the GW source is given by [164]

$$\sigma_{d_{\mathrm{L}}}^{\mathrm{pv}}(z) = d_{\mathrm{L}}(z)\times\left[1 + \frac{c(1+z)^2}{H(z)d_{\mathrm{L}}(z)}\right]\frac{\sqrt{\langle v^2\rangle}}{c}, \tag{15}$$

where c is the speed of light in vacuum, $H(z)$ is the Hubble parameter, and $\sqrt{\langle v^2\rangle}$ is the peculiar velocity of the GW

[7] There are several realistic candidates for the luminosity function of short GRB in recent studies, see [160] for more detailed discussions.

source with respect to the Hubble flow is roughly set to $\sqrt{\langle v^2 \rangle} = 500 \quad \mathrm{kms}^{-1}$.

Hence, the total error of d_{L} can be written as

$$\sigma_{d_{\mathrm{L}}} = \sqrt{(\sigma_{d_{\mathrm{L}}}^{\mathrm{inst}})^2 + (\sigma_{d_{\mathrm{L}}}^{\mathrm{lens}})^2 + (\sigma_{d_{\mathrm{L}}}^{\mathrm{pv}})^2}. \tag{16}$$

2.2. Other cosmological observations

For comparison, we also employ three current EM cosmological observations, i.e., the cosmic microwave background (CMB) data, the baryon acoustic oscillation (BAO) data, and the type Ia supernova (SN) data. The details of these data are listed as follows.

The CMB data: the CMB likelihood including the TT, TE, EE spectra at $l \geqslant 30$, the low-l temperature commander likelihood, and the low-l SimAll EE likelihood, from the Planck 2018 data release [165].

The BAO data: the measurements from 6dFGs at $z_{\mathrm{eff}} = 0.106$ [166], the SDSS-MGS at $z_{\mathrm{eff}} = 0.15$ [167], and BOSS-DR12 at $z_{\mathrm{eff}} = 0.38$, $z_{\mathrm{eff}} = 0.51$, and $z_{\mathrm{eff}} = 0.61$ [168].

The SN data: the Pantheon sample comprised of 1048 data points from the Pantheon compilation [169].

2.3. Methods of constraining cosmological parameters

In this paper, we will consider both cases of massless and massive sterile neutrinos in the framework of standard model (ΛCDM) of cosmology. For the ΛCDM model, the base parameter set (including six free parameters) is

$$\mathbf{P} = \{\omega_b, \quad \omega_c, \quad 100\theta_{\mathrm{MC}}, \quad \tau, \quad \ln(10^{10}A_{\mathrm{s}}), \quad n_{\mathrm{s}}\},$$

where $\omega_b \equiv \Omega_b h^2$ and $\omega_c \equiv \Omega_c h^2$ are the physical densities of baryon and cold dark matter, respectively, θ_{MC} is the ratio (multiplied by 100) between the sound horizon and the angular diameter distance at the time of last-scattering, τ is the optical depth to the reionization, A_{s} is the amplitude of the primordial curvature perturbation, and n_{s} is the scalar spectral index.

When we consider massless sterile neutrinos (as the dark radiation) in the ΛCDM model, an additional parameter N_{eff} (the effective number of relativistic species) need to be added in the model, and this case is called $\Lambda\mathrm{CDM}+N_{\mathrm{eff}}$ model in this paper. When the massive sterile neutrinos are considered in the ΛCDM model, two extra free parameters, the N_{eff} and $m_{\nu,\mathrm{sterile}}^{\mathrm{eff}}$ (the effective sterile neutrino mass) need to be added in the model, and this case is called $\Lambda\mathrm{CDM}+N_{\mathrm{eff}}+m_{\nu,\mathrm{sterile}}^{\mathrm{eff}}$ model in this paper. Thus, the $\Lambda\mathrm{CDM}+N_{\mathrm{eff}}$ model has seven independent parameters, and the $\Lambda\mathrm{CDM}+N_{\mathrm{eff}}+m_{\nu,\mathrm{sterile}}^{\mathrm{eff}}$ has eight independent parameters. Note that in both the massless and massive sterile neutrino cases the total mass of active neutrinos is fixed at $\sum m_\nu = 0.06$ eV.

For the GW standard siren observation with N data point, the χ^2 function is defined as

$$\chi^2_{\mathrm{GW}} = \sum_{i=1}^{N} \left[\frac{d_{\mathrm{L}}^i - d_{\mathrm{L}}(z_i; \overrightarrow{\Omega})}{\sigma_{d_{\mathrm{L}}}^i} \right]^2, \tag{17}$$

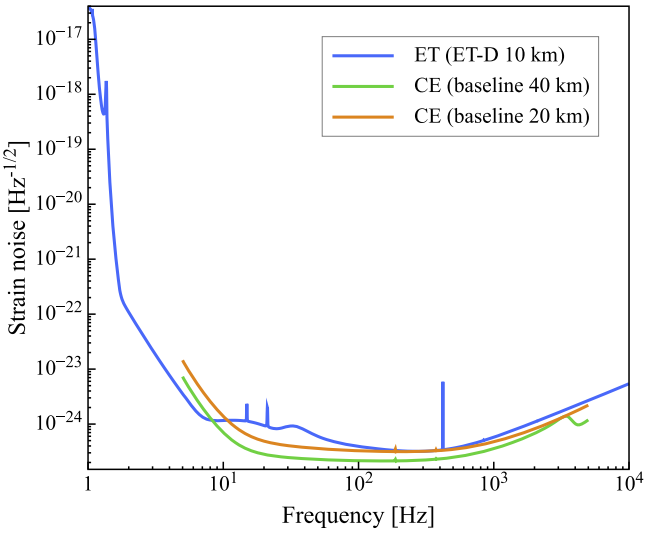

Figure 1. Sensitivity curves of the 3G GW detectors considered in this work.

Table 1. The specific coordinate parameters considered in this work.

GW detector	φ(deg)	λ(deg)	γ(deg)	ζ(deg)
Einstein Telescope, Europe	40.443	9.457	0.000	60
Cosmic Explorer, USA	43.827	−112.825	45.000	90
Cosmic Explorer, Australia	−34.000	145.000	90.000	90

where z_i, d_{L}^i, and $\sigma_{d_{\mathrm{L}}}^i$ are the i-th GW redshift, luminosity distance, and the measurement error of the luminosity distance, respectively, $\overrightarrow{\Omega}$ denotes the set of cosmological parameters.

In this work, we present the first forecast for the search for sterile neutrinos using joint GW-GRB observation. We use the public Markov-chain Monte Carlo (MCMC) package CosmoMC [170] to constrain sterile neutrino and other cosmological parameters. To demonstrate the impact of simulated GW data on constraining sterile neutrino parameters, we will consider all the different cases of 3G GW observations, the single ET, the single CE, the CE-CE network (one CE in the United States with 40-km arm length and another one in Australia with 20-km arm length, abbreviated as 2CE hereafter), and the ET-CE-CE network (one ET detector and two CE-like detectors, abbreviated as ET2CE hereafter) to analysis. We utilize the sensitivity curves of ET from [171] and for CE from [172], as shown in figure 1. For the GW detector, in view of the high uncertainty of the duty cycle, we only calculate the ideal scenario assuming a 100% duty cycle for all detectors, as discussed in [173]. The specific parameters characterizing the geometry of GW detector (latitude φ, longitude λ, opening angle ζ, and arm bisector angle γ) are detailed in table 1. The number of GW standard sirens in the subsequent cosmological analysis are shown in table 2 and their redshift distributions are shown in figure 2.

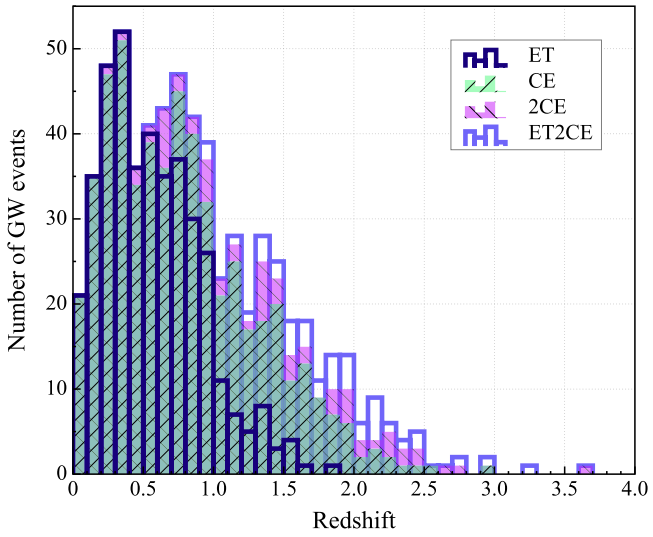

Figure 2. Redshift distributions of BNS detected by THESEUS in synergy with ET, CE, 2CE, and ET2CE for a 10-year observation.

Table 2. Numbers of GW standard sirens in cosmological analysis, triggered by THESEUS in synergy with ET, CE, 2CE, and ET2CE, respectively.

Detection strategy	ET	CE	2CE	ET2CE
Number of GW standard sirens	400	538	600	640

The primary goal of this work is to assess the influence of joint observations between 3G GW detectors and future GRB detectors on the cosmological measurement of sterile neutrino parameters. Such observations are crucial for alleviating the degeneracies in cosmological parameters that are commonly observed in traditional EM data. To elucidate this, we have conducted simulations to generate mock GW data, which we have subsequently integrated with the mainstream EM observations, i.e., CMB+BAO+SN data. Our analysis specifically focuses on the estimation errors and precision of sterile neutrino parameters derived from this combined dataset.

To avoid any inconsistencies in the cosmological parameters constrained by combining CMB+BAO+SN with GW mock data, we have adopted a strategic approach. This approach is designed to thoroughly investigate the capacity of GW mock data to break the parameter degeneracies present in conventional EM observations. For this purpose, we have utilized the best-fit values of the cosmological parameters derived from the CMB+BAO+SN dataset as the reference values for simulating the GW mock data corresponding to each cosmological model. This methodology enables a more accurate assessment of the role of GW data in enhancing the precision of parameter estimation and resolving the degeneracies encountered in traditional EM observations.

For simplicity, we use 'CBS' to denote the joint CMB +BAO+SN data combination. Thus, in our analysis, we use five data combinations: (1) CBS, (2) CBS+ET, (3) CBS+CE, (4) CBS+2CE, and (5) CBS+ET2CE. We will report the constraint results in the next section.

3. Results and discussion

In this section, we report the constraint results for the ΛCDM+$N_{\rm eff}$ and ΛCDM+$N_{\rm eff}$+$m^{\rm eff}_{\nu,\rm sterile}$ models using the CBS, CBS+ET, CBS+CE, CBS+2CE, and CBS+ET2CE data combinations and analyze how the GW standard sirens affect the cosmological constraints on the sterile neutrino parameters. The fitting results are shown in figures 3 and 4 and in tables 3 and 4. In the tables, we quote $\pm 1\sigma$ errors for the parameters, but for the parameters that cannot be well constrained, e.g., the sterile neutrino parameters $N_{\rm eff}$ and $m^{\rm eff}_{\nu,\rm sterile}$, we quote the 2σ upper limits. For a parameter ξ, we use $\sigma(\xi)$ and $\varepsilon(\xi)=\sigma(\xi)/\xi$ to represent its absolute error and relative error, respectively.

In accordance with the cosmological parameter constraints obtained from the CBS data, the central values and uncertainties of the cosmological parameters from the combined CBS and GW observations are detailed in tables 3 and 4. Given that the CBS data is real, whereas the GW data is simulated, the constraints from the joint CBS and GW analysis represent a mixture of real and simulated data. Consequently, the central values should not be interpreted as from actual observational data. As such, this work emphasizes the significance of the uncertainties and precision in the derived cosmological constraints.

3.1. The case of massless sterile neutrino

The massless sterile neutrinos serve as the dark radiation, and thus in this case $N_{\rm eff}$ is treated as a free parameter, the total relativistic energy density of radiation is given by

$$\rho_{\rm r}=\left[1+N_{\rm eff}\frac{7}{8}\left(\frac{4}{11}\right)^{\frac{4}{3}}\right]\rho_{\gamma}, \tag{18}$$

where ρ_{γ} is the photon energy density. In the ΛCDM model, $N_{\rm eff}=3.046$, and so $\Delta N_{\rm eff}=N_{\rm eff}-3.046>0$ indicates the presence of extra relativistic particle species in the early universe, and in this paper we take the fit results of $\Delta N_{\rm eff}>0$ as evidence of the existence of massless sterile neutrinos.

In table 3, we find that the CBS data provides only an upper limit, $N_{\rm eff}<3.464$, indicating that the existence of massless sterile neutrinos is not favored by the CBS data. However, when GW standard sirens are included in the data combination, the results change significantly. After considering the GW data, we obtain $N_{\rm eff}=3.209\pm0.060$ for CBS+ET, $N_{\rm eff}=3.209\pm0.056$ for CBS+CE, $N_{\rm eff}=3.210^{+0.055}_{-0.056}$ for CBS+2CE, and $N_{\rm eff}=3.208^{+0.054}_{-0.055}$ for CBS+ET2CE, which indicates a detection of $\Delta N_{\rm eff}>0$ at the 2.717σ, 2.911σ, 2.929σ, and 2.945σ significance levels, respectively. Obviously, the GW data can indeed effectively improve the constraints on the massless sterile neutrino parameter $N_{\rm eff}$.

Note that here CBS refers to current real observational data, while GW denotes simulated data. When we use the actual CBS data to conduct constraints, we can only obtain an upper limit for $N_{\rm eff}$ and not a definitive detection result. However, when simulated GW data is included, the errors in the parameter constraints are significantly reduced. With the

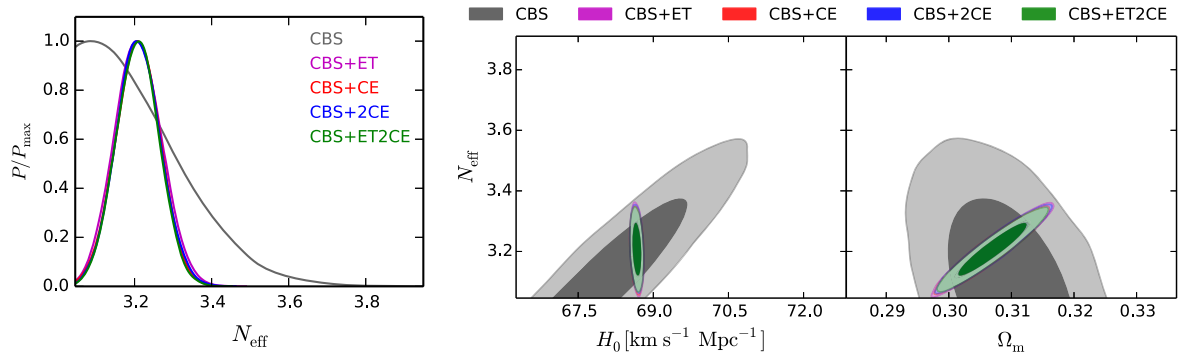

Figure 3. Constraint results for the ΛCDM+$N_{\rm eff}$ model from the CBS, CBS+ET, CBS+CE, CBS+2CE, and CBS+ET2CE data combinations. One-dimensional marginalized posterior distribution for $N_{\rm eff}$ (left panel), and two-dimensional marginalized posterior contours (1σ and 2σ) in the H_0–$N_{\rm eff}$ and Ω_m–$N_{\rm eff}$ planes (right panel).

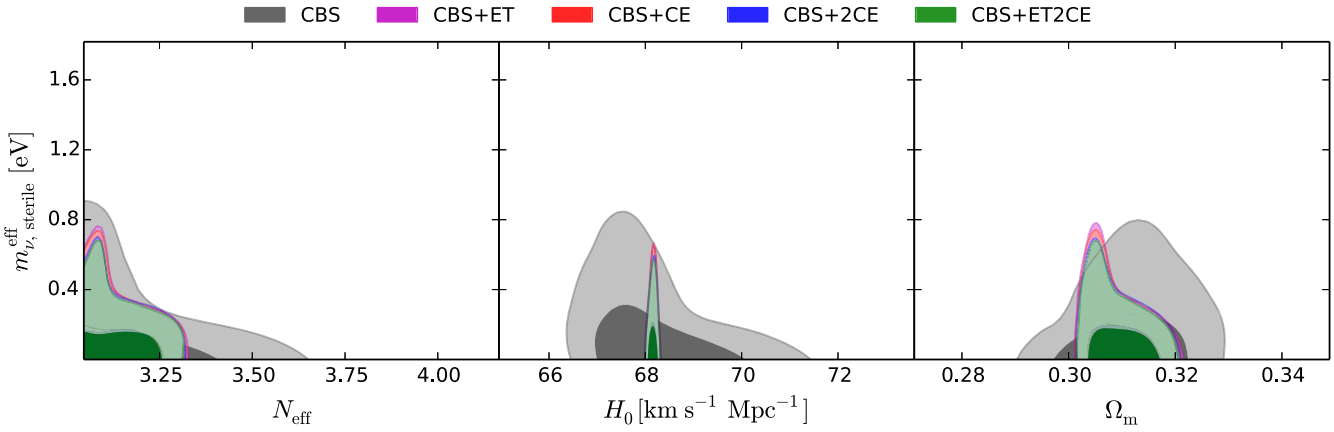

Figure 4. Two-dimensional marginalized posterior contours (1σ and 2σ) in the $N_{\rm eff}$–$m^{\rm eff}_{\nu,\rm sterile}$, H_0–$m^{\rm eff}_{\nu,\rm sterile}$, Ω_m–$m^{\rm eff}_{\nu,\rm sterile}$ planes for the ΛCDM+$N_{\rm eff}$+$m^{\rm eff}_{\nu,\rm sterile}$ model from the constraints of the CBS, CBS+ET, CBS+CE, CBS+2CE, and CBS+ET2CE data combinations.

Table 3. Fitting results of the ΛCDM+$N_{\rm eff}$ model by using the CBS, CBS+ET, CBS+CE, CBS+2CE, and CBS+ET2CE data combinations. We quote $\pm\ 1\sigma$ errors for the parameters, but for the parameters that cannot be well constrained, we quote the 2σ upper limits. Here, H_0 is in units of kms^{-1} Mpc^{-1}.

Model	CBS	CBS+ET	CBS+CE	CBS+2CE	CBS+ET2CE
$\Omega_b h^2$	0.02247 ± 0.00015	0.02248 ± 0.00011	0.02248 ± 0.00011	0.02248 ± 0.00011	0.02248 ± 0.00011
$\Omega_c h^2$	$0.1220^{+0.0017}_{-0.0028}$	0.1217 ± 0.0017	0.1217 ± 0.0016	0.1217 ± 0.0016	0.1217 ± 0.0016
$100\theta_{MC}$	$1.04046^{+0.00043}_{-0.00037}$	1.04050 ± 0.00036	$1.04050^{+0.00034}_{-0.00035}$	1.04049 ± 0.00035	1.04050 ± 0.00034
τ	$0.0558^{+0.0074}_{-0.0083}$	$0.0558^{+0.0075}_{-0.0082}$	$0.0559^{+0.0074}_{-0.0082}$	$0.0559^{+0.0075}_{-0.0082}$	$0.0558^{+0.0072}_{-0.0082}$
n_s	$0.9697^{+0.0046}_{-0.0057}$	0.9696 ± 0.0030	$0.9696^{+0.0030}_{-0.0031}$	0.9697 ± 0.0030	0.9697 ± 0.0029
$\ln(10^{10}A_s)$	$3.051^{+0.016}_{-0.018}$	3.050 ± 0.016	3.050 ± 0.016	3.050 ± 0.016	3.050 ± 0.016
σ_8	$0.8177^{+0.0083}_{-0.0101}$	$0.8170^{+0.0082}_{-0.0081}$	0.8169 ± 0.0078	0.8171 ± 0.0079	0.8169 ± 0.0077
Ω_m	$0.3077^{+0.0060}_{-0.0061}$	0.3071 ± 0.0038	$0.3071^{+0.0035}_{-0.0036}$	0.3071 ± 0.0035	$0.3070^{+0.0034}_{-0.0035}$
H_0	$68.670^{+0.640}_{-1.020}$	$68.671^{+0.057}_{-0.055}$	$68.671^{+0.056}_{-0.057}$	$68.671^{+0.052}_{-0.054}$	$68.672^{+0.052}_{-0.050}$
$N_{\rm eff}$	< 3.464	3.209 ± 0.060	3.209 ± 0.056	$3.210^{+0.055}_{-0.056}$	$3.208^{+0.054}_{-0.055}$
$\Delta N_{\rm eff} > 0$	...	2.717σ	2.911σ	2.929σ	2.945σ
$\sigma(\Omega_m)$	0.00605	0.00380	0.00355	0.00350	0.00345
$\sigma(H_0)$	0.8300	0.0560	0.0565	0.0530	0.0510
$\varepsilon(\Omega_m)$	1.966%	1.237%	1.156%	1.140%	1.124%
$\varepsilon(H_0)$	1.209%	0.082%	0.082%	0.077%	0.074%

central value of $N_{\rm eff}$ remaining essentially unchanged and $\Delta N_{\rm eff}$ substantially decreased, we can achieve a result of $\Delta N_{\rm eff} > 0$. Our results indicate that future GW observations can greatly assist in improving the cosmological detection of massless sterile neutrinos, with a significance level reaching up to 3σ. Of course, we must remember that our findings are based on simulated outcomes, and the central value of $N_{\rm eff}$ is set to be consistent with the result from CBS.

Table 4. Fitting results of the ΛCDM+$N_{\rm eff}$ + $m^{\rm eff}_{\nu,\rm sterile}$ model by using the CBS, CBS+ET, CBS+CE, CBS+2CE, and CBS+ET2CE data combinations. We quote $\pm 1\sigma$ errors for the parameters, but for the parameters that cannot be well constrained, we quote the 2σ upper limits. Here, H_0 is in units of kms^{-1}Mpc^{-1} and $m^{\rm eff}_{\nu,\rm sterile}$ is in units of eV.

Model	CBS	CBS+ET	CBS+CE	CBS+2CE	CBS+ET2CE
$\Omega_b h^2$	$0.02247^{+0.00015}_{-0.00016}$	0.02249 ± 0.00012	0.02249 ± 0.00012	0.02249 ± 0.00012	0.02249 ± 0.00012
$\Omega_c h^2$	$0.1198^{+0.0036}_{-0.0031}$	$0.1193^{+0.0033}_{-0.0018}$	$0.1193^{+0.0032}_{-0.0017}$	$0.1195^{+0.0031}_{-0.0017}$	$0.1194^{+0.0030}_{-0.0017}$
$100\theta_{MC}$	$1.04059^{+0.00047}_{-0.00033}$	$1.04071^{+0.00041}_{-0.00035}$	$1.04071^{+0.00040}_{-0.00035}$	$1.04070^{+0.00040}_{-0.00036}$	$1.04071^{+0.00039}_{-0.00036}$
τ	$0.0561^{+0.0073}_{-0.0083}$	$0.0566^{+0.0074}_{-0.0082}$	$0.0566^{+0.0074}_{-0.0082}$	$0.0568^{+0.0074}_{-0.0083}$	$0.0569^{+0.0074}_{-0.0083}$
n_s	$0.9681^{+0.0047}_{-0.0065}$	0.9684 ± 0.0033	0.9684 ± 0.0033	0.9684 ± 0.0033	$0.9684^{+0.0033}_{-0.0032}$
$\ln(10^{10}A_s)$	$3.048^{+0.016}_{-0.018}$	$3.048^{+0.016}_{-0.017}$	$3.048^{+0.016}_{-0.017}$	3.048 ± 0.016	3.048 ± 0.016
σ_8	$0.796^{+0.024}_{-0.014}$	$0.795^{+0.022}_{-0.012}$	$0.795^{+0.022}_{-0.012}$	$0.796^{+0.021}_{-0.012}$	$0.796^{+0.022}_{-0.012}$
Ω_m	0.3114 ± 0.0064	$0.3096^{+0.0032}_{-0.0052}$	$0.3096^{+0.0032}_{-0.0050}$	$0.3097^{+0.0033}_{-0.0049}$	$0.3096^{+0.0033}_{-0.0048}$
H_0	$68.150^{+0.500}_{-1.000}$	$68.156^{+0.055}_{-0.053}$	$68.156^{+0.054}_{-0.053}$	$68.156^{+0.054}_{-0.053}$	$68.156^{+0.054}_{-0.050}$
$N_{\rm eff}$	< 3.446	$3.148^{+0.039}_{-0.094}$	$3.148^{+0.040}_{-0.090}$	$3.150^{+0.043}_{-0.089}$	$3.150^{+0.042}_{-0.089}$
$m^{\rm eff}_{\nu,\rm sterile}$	< 0.5789	< 0.4842	< 0.4772	< 0.4321	< 0.4226
$\Delta N_{\rm eff} > 0$	...	1.085σ	1.133σ	1.169σ	1.169σ
$\sigma(\Omega_m)$	0.00640	0.00420	0.00410	0.00410	0.00405
$\sigma(H_0)$	0.7500	0.0540	0.0535	0.0535	0.0520
$\varepsilon(\Omega_m)$	2.055%	1.357%	1.324%	1.324%	1.308%
$\varepsilon(H_0)$	1.101%	0.079%	0.078%	0.078%	0.076%

In the right panel of figure 3, we show the two-dimensional posterior distribution contours (1σ and 2σ) in the $N_{\rm eff}$–H_0 and $N_{\rm eff}$–Ω_m planes for the ΛCDM+$N_{\rm eff}$ model using CBS, CBS+ET, CBS+CE, CBS+2CE, and CBS+ET2CE data combinations. We can see that $N_{\rm eff}$ is in positive correlation with H_0 by using the CBS data combination. However, after adding the GW data, this correlation becomes negligible, indicating that the degeneracy between $N_{\rm eff}$ and H_0 is effectively broken by the GW observations. In addition, we can also clearly see that when considering the GW data, the parameter space is greatly shrunk in each plane and the constraints on cosmological parameters of H_0 and Ω_m become much tighter.

In table 3, we also show absolute and relative errors of H_0 and Ω_m from the CBS, CBS+ET, CBS+CE, CBS+2CE, and CBS+ET2CE data combinations. Compared to the CBS data, we find that the accuracy of the H_0 constraint improves by 93.253% for CBS+ET, 93.193% for CBS+CE, 93.614% for CBS+2CE, and 93.855% for CBS+ET2CE, respectively. Similarly, the accuracy of the Ω_m constraint improves by 37.190% for CBS+ET, 41.322% for CBS+CE, 42.149% for CBS+2CE, and 42.975% for CBS+ET2CE, respectively. Obviously, the GW data can indeed effectively improve the constraints on the parameters H_0 and Ω_m.

3.2. The case of massive sterile neutrino

In this subsection, we investigated how GW standard sirens constrain the massive sterile neutrino parameters. Hence, the requirement of $N_{\rm eff} > 3.046$ still holds.

From table 4, we obtain $N_{\rm eff} < 3.446$ by using CBS data. After adding the GW data, the constraint results become $N_{\rm eff} = 3.148^{+0.039}_{-0.094}$ for CBS+ET, $N_{\rm eff} = 3.148^{+0.039}_{-0.090}$ for CBS+CE, $N_{\rm eff} = 3.150^{+0.043}_{-0.089}$ for CBS+2CE, and $N_{\rm eff} = 3.150^{+0.042}_{-0.089}$ for CBS+ET2CE, respectively. We find that $N_{\rm eff}$ cannot be well constrained using the CBS data, but the addition of GW data can significantly improve the constraint on $N_{\rm eff}$, favoring $\Delta N_{\rm eff} > 0$ at 1.085σ (CBS+ET), 1.133σ (CBS+CE), 1.169σ (CBS+2CE), and 1.169σ (CBS+ET2CE) statistical significance, respectively. For the mass of sterile neutrino, the CBS data give $m^{\rm eff}_{\nu,\rm sterile} < 0.5789$ eV and further including the GW data leads to results of $m^{\rm eff}_{\nu,\rm sterile} < 0.4842$ eV (CBS+ET), $m^{\rm eff}_{\nu,\rm sterile} < 0.4772$ eV (CBS+CE), $m^{\rm eff}_{\nu,\rm sterile} < 0.4321$ eV (CBS+2CE), and $m^{\rm eff}_{\nu,\rm sterile} < 0.4226$ eV (CBS+ET2CE), respectively. Evidently, adding GW data tightens the constraint on $m^{\rm eff}_{\nu,\rm sterile}$ significantly, which is in accordance with the conclusions in previous studies' active neutrinos mass by using the GW data [14, 37, 46]. Therefore, the GW data also plays an important role in constraining the mass of sterile neutrinos.

In figure 4, we show two-dimensional marginalized posterior contours (1σ and 2σ) in the $N_{\rm eff}$–$m^{\rm eff}_{\nu,\rm sterile}$, H_0–$m^{\rm eff}_{\nu,\rm sterile}$, Ω_m–$m^{\rm eff}_{\nu,\rm sterile}$ planes for the ΛCDM+$N_{\rm eff}$+$m^{\rm eff}_{\nu,\rm sterile}$ model. We can clearly see that when further considering the GW data, the parameter space is also greatly shrunk and the constraints on H_0 and Ω_m also become much tighter. From table 4, we find that the constraints on H_0 and Ω_m could be improved by 92.800% and 34.375%, respectively, when adding the ET data to the CBS data, 92.867% and 35.938% for the case of CE, 92.867% and 35.938% for the case of 2CE, and 93.067% and 36.719% for the case of ET2CE, respectively. These results are in accordance with the conclusions for both the case of massless sterile neutrinos in this study and active neutrinos mass in previous studies [14, 37, 46]. Therefore, the inclusion of GW data can significantly improve constraints on most cosmological parameters, particularly H_0 and Ω_m.

4. Conclusion

This work aims to forecast the search for sterile neutrinos using joint GW-GRB observations. We consider two cases of massless and massive sterile neutrinos, corresponding to the ΛCDM+$N_{\rm eff}$ and ΛCDM+$N_{\rm eff}$+$m^{\rm eff}_{\nu,{\rm sterile}}$ models, respectively. We consider four GW detection observation strategies, i.e., ET, CE, the 2CE network, and the ET2CE network, to perform cosmological analysis. To evaluate the impact of GW data on the constraints of sterile neutrino parameters, we also considered existing CMB+BAO+SN data for comparison and combination.

For the ΛCDM+$N_{\rm eff}$ model, in the case of using CMB +BAO+SN, only upper limits on $N_{\rm eff}$ can be obtained. Further adding the GW data tightens the $N_{\rm eff}$ significantly, and in this case the preference of $\Delta N_{\rm eff} > 0$ at about 3σ level. Therefore, GW standard siren observations can greatly assist in the detection of massless sterile neutrinos.

For the ΛCDM+$N_{\rm eff}$+$m^{\rm eff}_{\nu,{\rm sterile}}$ model, only upper limits on $N_{\rm eff}$ and $m^{\rm eff}_{\nu,{\rm sterile}}$ can be derived by using the CMB+BAO +SN data. Further including GW data significantly improves the constraints, and we find that the GW data gives a rather tight upper limit on $m^{\rm eff}_{\nu,{\rm sterile}}$ and favor $\Delta N_{\rm eff} > 0$ at about 1.1σ level. These results also seem to favor massless sterile neutrinos.

Furthermore, we find that the GW data can significantly enhance the accuracy of constraints on the derived parameters H_0 and Ω_m. The accuracy of H_0 improves by approximately 93% and the accuracy of Ω_m increases by about 37% to 42%, when the GW data is included in the cosmological fit.

Acknowledgments

This work was supported by the National Natural Science Foundation of China under Grant Nos. 12305069, 11947022, 12473001, 11975072, 11875102, and 11835009, the National SKA Program of China under Grants Nos. 2022SKA0110200 and 2022SKA0110203, the Program of the Education Department of Liaoning Province under Grant No. JYTMS20231695, and the National 111 Project under Grant No. B16009.

References

[1] Abbott B P *et al* 2017 GW170817: Observation of gravitational waves from a binary neutron star inspiral *Phys. Rev. Lett.* **119** 161101
[2] Abbott B P *et al* 2017 Multi-messenger observations of a binary neutron star merger *Astrophys. J. Lett.* **848** l12
[3] Dìaz M C *et al* 2017 Observations of the first electromagnetic counterpart to a gravitational wave source by the TOROS collaboration *Astrophys. J. Lett.* **848** l29
[4] ET https://www.et-gw.eu/
[5] Punturo M *et al* 2010 The Einstein telescope: A third-generation gravitational wave observatory *Class. Quant. Grav.* **27** 194002
[6] CE https://cosmicexplorer.org/
[7] Benjamin P *et al* 2017 Exploring the sensitivity of next generation gravitational wave detectors *Class. Quant. Grav* **34** 044001
[8] Cai R-G and Yang T 2017 Estimating cosmological parameters by the simulated data of gravitational waves from the Einstein Telescope *Phys. Rev.* D **95** 044024
[9] Cai R-G and Yang T 2018 Standard sirens and dark sector with Gaussian process *EPJ Web Conf.* **168** 01008
[10] Liu T, Zhang X and Zhao W 2018 Constraining $f(R)$ gravity in solar system, cosmology and binary pulsar systems *Phys. Lett.* B **777** 286293
[11] Cai R-G, Liu T-B, Liu X-W, Wang S-J and Yang T 2018 Probing cosmic anisotropy with gravitational waves as standard sirens *Phys. Rev.* D **97** 103005
[12] Berti E, Yagi K and Yunes N 2018 Extreme gravity tests with gravitational waves from compact binary coalescences: (I) inspiral-merger *Gen. Rel. Grav.* **50** 46
[13] Cai Y-F, Li C, Saridakis E N and Xue L 2018 $f(T)$ gravity after GW170817 and GRB170817A *Phys. Rev.* D **97** 103513
[14] Wang L-F, Zhang X-N, Zhang J-F and Zhang X 2018 Impacts of gravitational-wave standard siren observation of the Einstein Telescope on weighing neutrinos in cosmology *Phys. Lett.* B **782** 87–93
[15] Zhao W, Wright B S and Li B 2018 Constraining the time variation of Newton's constant G with gravitational-wave standard sirens and supernovae *J. Cosmol. Astropart. Phys.* **2018** 052
[16] Zhang X-N, Wang L-F, Zhang J-F and Zhang X 2019 Improving cosmological parameter estimation with the future gravitational-wave standard siren observation from the Einstein Telescope *Phys. Rev.* D **99** 063510
[17] Du M, Yang W, Xu L, Pan S and Mota D F 2019 Future constraints on dynamical dark-energy using gravitational-wave standard sirens *Phys. Rev.* D **100** 043535
[18] He J-H 2019 Accurate method to determine the systematics due to the peculiar velocities of galaxies in measuring the Hubble constant from gravitational-wave standard sirens *Phys. Rev.* D **100** 023527
[19] Yang W, Pan S, Valentino E D, Wang B and Wang A 2020 Forecasting interacting vacuum-energy models using gravitational waves *J. Cosmol. Astropart. Phys.* **2020** 050
[20] Yang W, Vagnozzi S, Valentino E D, Nunes R C, Pan S and Mota D F 2019 Listening to the sound of dark sector interactions with gravitational wave standard sirens *J. Cosmol. Astropart. Phys.* **2019** 037
[21] Zhang X 2019 Gravitational wave standard sirens and cosmological parameter measurement *Sci. China Phys. Mech. Astron.* **62** 110431
[22] Zhang J-F, Dong H-Y, Qi J-Z and Zhang X 2020 Prospect for constraining holographic dark energy with gravitational wave standard sirens from the Einstein Telescope *Eur. Phys. J.* C **80** 217
[23] Bachega R R A, Costa A A, Abdalla E and Fornazier K S F 2020 Forecasting the interaction in dark matter-dark energy models with standard sirens from the Einstein Telescope *J. Cosmol. Astropart. Phys.* **2020** 021
[24] Wang L-F, Zhao Z-W, Zhang J-F and Zhang X 2020 A preliminary forecast for cosmological parameter estimation with gravitational-wave standard sirens from TianQin *J. Cosmol. Astropart. Phys.* **2020** 012
[25] Zhang J-F, Zhang M, Jin S-J, Qi J-Z and Zhang X 2019 Cosmological parameter estimation with future gravitational wave standard siren observation from the Einstein Telescope *J. Cosmol. Astropart. Phys.* **2019** 068
[26] Li H-L, He D-Z, Zhang J-F and Zhang X 2020 Quantifying the impacts of future gravitational-wave data on constraining interacting dark energy *J. Cosmol. Astropart. Phys.* **2020** 038

[27] Zhao Z-W, Wang L-F, Zhang J-F and Zhang X 2020 Prospects for improving cosmological parameter estimation with gravitational-wave standard sirens from Taiji *Sci. Bull.* **65** 1340–8

[28] Jin S-J, He D-Z, Xu Y, Zhang J-F and Zhang X 2020 Forecast for cosmological parameter estimation with gravitational-wave standard siren observation from the Cosmic Explorer *J. Cosmol. Astropart. Phys.* **2020** 051

[29] Wang L-F, Jin S-J, Zhang J-F and Zhang X 2022 Forecast for cosmological parameter estimation with gravitational-wave standard sirens from the LISA-Taiji network *Sci. China Phys. Mech. Astron.* **65** 210411

[30] Qi J-Z, Jin S-J, Fan X-L, Zhang J-F and Zhang X 2021 Using a multi-messenger and multi-wavelength observational strategy to probe the nature of dark energy through direct measurements of cosmic expansion history *J. Cosmol. Astropart. Phys.* **2021** 042

[31] Jin S-J, Wang L-F, Wu P-J, Zhang J-F and Zhang X 2021 How can gravitational-wave standard sirens and 21-cm intensity mapping jointly provide a precise late-universe cosmological probe? *Phys. Rev.* D **104** 103507

[32] Zhu L-G, Xie L-H, Hu Y-M, Liu S, Li E-K, Napolitano N R, Tang B-T, Zhang J and Mei J 2022 Constraining the Hubble constant to a precision of about 1% using multi-band dark standard siren detections *Sci. China Phys. Mech. Astron.* **65** 259811

[33] Mendonça J, de Souza S, Sturani R and Alcaniz J 2022 Cosmography with standard sirens from the Einstein Telescope *J. Cosmol. Astropart. Phys.* **2022** 025

[34] Wang L-F, Shao Y, Zhang J-F and Zhang X 2022 Ultra-low-frequency gravitational waves from individual supermassive black hole binaries as standard sirens arXiv:2201.00607

[35] Wu P-J, Shao Y, Jin S-J and Zhang X 2023 A path to precision cosmology: synergy between four promising late-universe cosmological probes *J. Cosmol. Astropart. Phys.* **06** 052

[36] Jin S-J, Li T-N, Zhang J-F and Zhang X 2023 Prospects for measuring the Hubble constant and dark energy using gravitational-wave dark sirens with neutron star tidal deformation *J. Cosmol. Astropart. Phys.* **2023** 070

[37] Jin S-J, Zhu R-Q, Wang L-F, Li H-L, Zhang J-F and Zhang X 2022 Impacts of gravitational-wave standard siren observations from Einstein Telescope and Cosmic Explorer on weighing neutrinos in interacting dark energy models *Commun. Theor. Phys.* **74** 105404

[38] Hou W-T, Qi J-Z, Han T, Zhang J-F, Cao S and Zhang X 2023 Prospects for constraining interacting dark energy models from gravitational wave and gamma ray burst joint observation *J. Cosmol. Astropart. Phys.* **2023** 017

[39] Song J-Y, Wang L-F, Li Y, Zhao Z-W, Zhang J-F, Zhao W and Zhang X 2024 Synergy between CSST galaxy survey and gravitational-wave observation: inferring the Hubble constant from dark standard sirens *Sci. China Phys. Mech. Astron.* **67** 230411

[40] Jin S-J, Xing S-S, Shao Y, Zhang J-F and Zhang X 2023 Joint constraints on cosmological parameters using future multi-band gravitational wave standard siren observations *Chin. Phys.* C **47** 065104

[41] Jin S-J, Zhang Y-Z, Song J-Y, Zhang J-F and Zhang X 2024 Taiji-TianQin-LISA network: precisely measuring the Hubble constant using both bright and dark sirens *Sci. China Phys. Mech. Astron.* **67** 220412

[42] Jin S-J, Zhu R-Q, Song J-Y, Han T, Zhang J-F and Zhang X 2023 Standard siren cosmology in the era of the 2.5-generation ground-based gravitational wave detectors: bright and dark sirens of LIGO Voyager and NEMO *J. Cosmol. Astropart. Phys.* **2024** 050

[43] Han T, Jin S-J, Zhang J-F and Zhang X 2024 A comprehensive forecast for cosmological parameter estimation using joint observations of gravitational waves and short -ray bursts *Eur. Phys. J.* C **84** 663

[44] Li T-N, Jin S-J, Li H-L, Zhang J-F and Zhang X 2024 Prospects for probing the interaction between dark energy and dark matter using gravitational-wave dark sirens with neutron star tidal deformation *Astrophys. J.* **963** 52

[45] Dong Y-Y, Song J-Y, Jin S-J, Zhang J-F and Zhang X 2024 Enhancing dark siren cosmology through multi-band gravitational wave synergetic observations arXiv:2404.18188

[46] Feng L, Han T, Zhang J-F and Zhang X 2024 Prospects for weighing neutrinos in interacting dark energy models using joint observations of gravitational waves and γ-ray bursts *Chin. Phys.* C **48** 095104

[47] Bian L *et al* 2021 The gravitational-wave physics II: progress *Sci. China Phys. Mech. Astron.* **64** 120401

[48] Aguilar A *et al* 2001 Evidence for neutrino oscillations from the observation of $\bar{\nu}_e$ appearance in a $\bar{\nu}_e$ beam *Phys. Rev.* D **64** 112007

[49] Giunti C and Laveder M 2011 Statistical significance of the gallium anomaly *Phys. Rev.* C **83** 065504

[50] Akbar M, Quevedo H, Saifullah K, Sanchez A and Taj S 2011 Thermodynamic geometry of charged rotating BTZ black holes *Phys. Rev.* D **83** 084031

[51] Conrad J M, Ignarra C M, Karagiorgi G, Shaevitz M H and Spitz J 2013 Sterile neutrino fits to short baseline neutrino oscillation measurements *Adv. High Energy Phys.* **163897** 2013

[52] Aguilar-Arevalo A A *et al* 2012 A combined $\nu_\mu \to \nu_e$ and $\bar{\nu}_\mu \to \bar{\nu}_e$ oscillation analysis of the MiniBooNE excesses arXiv:1207.4809

[53] Giunti C, Laveder M, Li Y F, Liu Q Y and Long H W 2012 Update of short-baseline electron neutrino and antineutrino disappearance *Phys. Rev.* D **86** 113014

[54] Giunti C, Laveder M, Li Y F and Long H W 2013 Short-baseline electron neutrino oscillation length after troitsk *Phys. Rev.* D **87** 013004

[55] Kopp J, Machado P A N, Maltoni M and Schwetz T 2013 Sterile neutrino oscillations: the global picture *J. High Energy Phys.* **05** 050

[56] Giunti C, Laveder M, Li Y F and Long H W 2013 Pragmatic view of short-baseline neutrino oscillations *Phys. Rev.* D **88** 073008

[57] Gariazzo S, Giunti C and Laveder M 2013 Light sterile neutrinos in cosmology and short-baseline oscillation experiments *J. High Energy Phys.* **2013** JHEP11(2013)211

[58] Abazajian K N *et al* 2012 Light sterile neutrinos: a white paper arXiv:1204.5379

[59] Hannestad S, Tamborra I and Tram T 2012 Thermalisation of light sterile neutrinos in the early Universe *J. Cosmol. Astropart. Phys.* **2012** 025

[60] Conrad J M, Louis W C and Shaevitz M H 2012 The LSND and MiniBooNE oscillation searches at high Δm^2 *Ann. Rev. Nucl. Part. Sci.* **63** 4567

[61] Hu W, Eisenstein D J and Tegmark M 1998 Weighing neutrinos with galaxy surveys *Phys. Rev. Lett.* **80** 5255–8

[62] Reid B A, Verde L, Jimenez R and Mena O 2010 Robust neutrino constraints by combining low redshift observations with the CMB *J. Cosmol. Astropart. Phys.* **2010** 003

[63] Li H and Zhang X 2012 Constraining dynamical dark energy with a divergence-free parametrization in the presence of spatial curvature and massive neutrinos *Phys. Lett.* B **713** 160–4

[64] Wang X, Meng X-L, Zhang T-J, Shan H Y, Gong Y, Tao C, Chen X and Huang Y F 2012 Observational constraints on cosmic neutrinos and dark energy revisited *J. Cosmol. Astropart. Phys.* **2012** 018

[65] Hamann J, Hannestad S and Wong Y Y Y 2012 Measuring neutrino masses with a future galaxy survey *J. Cosmol. Astropart. Phys.* **2012** 052

[66] Li Y-H, Wang S, Li X-D and Zhang X 2013 Holographic dark energy in a Universe with spatial curvature and massive neutrinos: a full Markov Chain Monte Carlo exploration *J. Cosmol. Astropart. Phys.* **02** 033

[67] Riemer-Sørensen S, Parkinson D and Davis T M 2014 Combining Planck data with large scale structure information gives a strong neutrino mass constraint *Phys. Rev.* D **89** 103505

[68] Giusarma E, de Putter R, Ho S and Mena O 2013 Constraints on neutrino masses from Planck and Galaxy clustering data *Phys. Rev.* D **88** 063515

[69] Cahn R N, Dwyer D A, Freedman S J, Haxton W C, Kadel R W, Kolomensky Y G, Luk K B, McDonald P, Orebi Gann G D and Poon A W P 2013 White paper: measuring the neutrino mass hierarchy arXiv:1307.5487

[70] Lesgourgues J and Pastor S 2014 Neutrino cosmology and Planck *New J. Phys.* **16** 065002

[71] Zhang J-F, Li Y-H and Zhang X 2014 Cosmological constraints on neutrinos after BICEP2 *Eur. Phys. J.* C **74** 2954

[72] Zhou X-Y and He J-H 2014 Weighing neutrinos in $f(R)$ gravity in light of BICEP2 *Commun. Theor. Phys.* **62** 102108

[73] Costanzi M, Sartoris B, Viel M and Borgani S 2014 Neutrino constraints: what large-scale structure and CMB data are telling us? *J. Cosmol. Astropart. Phys.* **2014** 081

[74] Nathalie P-D *et al* 2014 Constraint on neutrino masses from SDSS-III/BOSS Lyα forest and other cosmological probes *J. Cosmol. Astropart. Phys.* **02** 045

[75] Zhang J-F, Zhao M-M, Li Y-H and Zhang X 2015 Neutrinos in the holographic dark energy model: constraints from latest measurements of expansion history and growth of structure *J. Cosmol. Astropart. Phys.* **04** 038

[76] Qian X and Vogel P 2015 Neutrino mass hierarchy *Prog. Part. Nucl. Phys.* **83** 1–30

[77] Patterson R B 2015 Prospects for measurement of the neutrino mass hierarchy *Ann. Rev. Nucl. Part. Sci.* **65** 177–92

[78] Allison R, Caucal P, Calabrese E, Dunkley J and Louis T 2015 Towards a cosmological neutrino mass detection *Phys. Rev.* D **92** 123535

[79] Geng C-Q, Lee C-C, Myrzakulov R, Sami M and Saridakis E N 2016 Observational constraints on varying neutrino-mass cosmology *J. Cosmol. Astropart. Phys.* **2016** 049

[80] Chen Y and Xu L 2016 Galaxy clustering, CMB and supernova data constraints on ϕ CDM model with massive neutrinos *Phys. Lett.* B **752** 6675

[81] Zhang X 2015 Impacts of dark energy on weighing neutrinos after Planck *Phys. Rev.* D **93** 083011

[82] Huang Q-G, Wang K and Wang S 2016 Constraints on the neutrino mass and mass hierarchy from cosmological observations *Eur. Phys. J.* C **76** 489

[83] Chen Y, Ratra B, Biesiada M, Li S and Zhu Z-H 2016 Constraints on non-flat cosmologies with massive neutrinos after Planck 2015 *Astrophys. J.* **829** 61

[84] Moresco M, Jimenez R, Verde L, Cimatti A, Pozzetti L, Maraston C and Thomas D 2016 Constraining the time evolution of dark energy, curvature and neutrino properties with cosmic chronometers *J. Comsol. Astropart. Phys.* **2016** 039

[85] Lu J, Liu M, Wu Y, Wang Y and Yang W 2016 Cosmic constraint on massive neutrinos in viable $f(R)$ gravity with producing ΛCDM background expansion *Eur. Phys. J.* C **76** 679

[86] Hada R and Futamase T 2016 Constraints on neutrino masses from the lensing dispersion of Type Ia supernovae *Astrophys. J.* **828** 112

[87] Wang S, Wang Y-F, Xia D-M and Zhang X 2016 Impacts of dark energy on weighing neutrinos: mass hierarchies considered *Phys. Rev.* D **94** 083519

[88] Kumar S and Nunes R C 2016 Probing the interaction between dark matter and dark energy in the presence of massive neutrinos *Phys. Rev.* D **94** 123511

[89] Zhao M-M, Li Y-H, Zhang J-F and Zhang X 2016 Constraining neutrino mass and extra relativistic degrees of freedom in dynamical dark energy models using Planck 2015 data in combination with low-redshift cosmological probes: basic extensions to ΛCDM cosmology *Mon. Not. Roy. Astron. Soc.* **469** 17131724

[90] Böhringer H and Chon G 2016 Constraints on neutrino masses from the study of the nearby large-scale structure and galaxy cluster counts *Mod. Phys. Lett.* A **31** 1640008

[91] Xu L and Huang Q-G 2018 Detecting the neutrinos mass hierarchy from cosmological data *Sci. China Phys. Mech. Astron.* **61** 039521

[92] Vagnozzi S, Giusarma E, Mena O, Freese K, Gerbino M, Ho S and Lattanzi M 2017 Unveiling ν secrets with cosmological data: neutrino masses and mass hierarchy *Phys. Rev.* D **96** 123503

[93] Guo R-Y, Li Y-H, Zhang J-F and Zhang X 2017 Weighing neutrinos in the scenario of vacuum energy interacting with cold dark matter: application of the parameterized post-Friedmann approach *J. Cosmol. Astropart. Phys.* **05** 040

[94] Zhang X 2017 Weighing neutrinos in dynamical dark energy models *Sci. China Phys. Mech. Astron.* **60** 060431

[95] Chen L, Huang Q-G and Wang K 2017 New cosmological constraints with extended-Baryon Oscillation Spectroscopic Survey DR14 quasar sample *Eur. Phys. J.* C **77** 762

[96] Yang W, Nunes R C, Pan S and Mota D F 2017 Effects of neutrino mass hierarchies on dynamical dark energy models *Phys. Rev.* D **95** 103522

[97] Koksbang S M and Hannestad S 2017 Constraining dynamical neutrino mass generation with cosmological data *J. Cosmol. Astropart. Phys.* **2017** 014

[98] Li E-K, Zhang H, Du M, Zhou Z-H and Xu L 2018 Probing the neutrino mass hierarchy beyond ΛCDM model *J. Cosmol. Astropart. Phys.* **2018** 042

[99] Wang S, Wang Y-F and Xia D-M 2018 Constraints on the sum of neutrino masses using cosmological data including the latest extended Baryon Oscillation Spectroscopic Survey DR14 quasar sample *Chin. Phys.* C **42** 065103

[100] Zhao M-M, Zhang J-F and Zhang X 2018 Measuring growth index in a universe with massive neutrinos: a revisit of the general relativity test with the latest observations *Phys. Lett.* B **779** 473–8

[101] Boyle A and Komatsu E 2018 Deconstructing the neutrino mass constraint from galaxy redshift surveys *J. Comsol. Astropart. Phys.* **2018** 035

[102] Vagnozzi S, Dhawan S, Gerbino M, Freese K, Goobar A and Mena O 2018 Constraints on the sum of the neutrino masses in dynamical dark energy models with $w(z) \geqslant -1$ are tighter than those obtained in ΛCDM *Phys. Rev.* D **98** 083501

[103] Guo R-Y, Zhang J-F and Zhang X 2018 Exploring neutrino mass and mass hierarchy in the scenario of vacuum energy interacting with cold dark matte. *Chin. Phys.* C **42** 095103

[104] Choudhury S R and Choubey S 2018 Updated bounds on sum of neutrino masses in various cosmological scenarios *J. Comsol. Astropart. Phys.* **2018** 017

[105] Feng L, Li H-L, Zhang J-F and Zhang X 2020 Exploring neutrino mass and mass hierarchy in interacting dark energy models *Sci. China Phys. Mech. Astron.* **63** 220401

[106] Zhang J-F, Wang B and Zhang X 2020 Forecast for weighing neutrinos in cosmology with SKA *Sci. China Phys. Mech. Astron.* **63** 280411

[107] Li H-L, Zhang J-F and Zhang X 2018 Constraints on neutrino mass in the scenario of vacuum energy interacting with cold dark matter after Planck *Commun. Theor. Phys.* **72** 125401

[108] Zhang M, Zhang J-F and Zhang X 2020 Impacts of dark energy on constraining neutrino mass after Planck 2018 *Commun. Theor. Phys.* **72** 125402
[109] de Holanda P C and Smirnov A Y 2011 Solar neutrino spectrum, sterile neutrinos and additional radiation in the Universe *Phys. Rev.* D **83** 113011
[110] Palazzo A 2013 Phenomenology of light sterile neutrinos: a brief review *Mod. Phys. Lett.* A **28** 1330004
[111] Hamann J and Hasenkamp J 2013 A new life for sterile neutrinos: resolving inconsistencies using hot dark matter *J. Cosmol. Astropart. Phys.* **10** 044
[112] Wyman M, Rudd D H, Vanderveld R A and Hu W 2014 Neutrinos help reconcile Planck measurements with the local Universe *Phys. Rev. Lett.* **112** 051302
[113] Battye R A and Moss A 2014 Evidence for massive neutrinos from cosmic microwave background and lensing observations *Phys. Rev. Lett.* **112** 051303
[114] Dvorkin C, Wyman M, Rudd D H and Hu W 2014 Neutrinos help reconcile Planck measurements with both the early and local Universe *Phys. Rev.* D **90** 083503
[115] Archidiacono M, Fornengo N, Gariazzo S, Giunti C, Hannestad S and Laveder M 2014 Light sterile neutrinos after BICEP-2 *J. Cosmol. Astropart. Phys.* **2014** 031
[116] Ko P and Tang Y 2014 $\nu\Lambda$MDM: A model for sterile neutrino and dark matter reconciles cosmological and neutrino oscillation data after BICEP2 *Phys. Lett.* B **739** 6267
[117] Li Y-H, Zhang J-F and Zhang X 2014 Tilt of primordial gravitational wave spectrum in a universe with sterile neutrinos *Sci. China Phys. Mech. Astron.* **57** 1455–9
[118] Zhang J-F, Li Y-H and Zhang X 2015 Sterile neutrinos help reconcile the observational results of primordial gravitational waves from Planck and BICEP2 *Phys. Lett.* B **740** 359–63
[119] Archidiacono M, Hannestad S, Hansen R S and Tram T 2015 Cosmology with self-interacting sterile neutrinos and dark matter - A pseudoscalar model *Phys. Rev.* D **91** 065021
[120] Bergström J, Gonzalez-Garcia M C, Niro V and Salvado J 2014 Statistical tests of sterile neutrinos using cosmology and short-baseline data *J. High Energy Phys.* **2014** JHEP10 (2014)104
[121] An F P *et al* 2014 Search for a light sterile neutrino at daya bay *Phys. Rev. Lett.* **113** 141802
[122] Zhang J-F, Geng J-J and Zhang X 2014 Neutrinos and dark energy after Planck and BICEP2: data consistency tests and cosmological parameter constraints *J. Cosmol. Astropart. Phys.* **10** 044
[123] Zhang J-F, Li Y-H and Zhang X 2014 Measuring growth index in a universe with sterile neutrinos *Phys. Lett.* B **739** 102–5
[124] Li Y-H, Zhang J-F and Zhang X 2015 Probing $f(R)$ cosmology with sterile neutrinos via measurements of scale-dependent growth rate of structure *Phys. Lett.* B **744** 213–7
[125] Feng L, Zhang J-F and Zhang X 2017 A search for sterile neutrinos with the latest cosmological observations *Eur. Phys. J.* C **77** 418
[126] Zhao M-M, He D-Z, Zhang J-F and Zhang X 2017 Search for sterile neutrinos in holographic dark energy cosmology: Reconciling Planck observation with the local measurement of the Hubble constant *Phys. Rev.* D **96** 043520
[127] Feng L, Zhang J-F and Zhang X 2018 Searching for sterile neutrinos in dynamical dark energy cosmologies *Sci. China Phys. Mech. Astron.* **61** 050411
[128] Feng L, Zhang J-F and Zhang X 2019 Search for sterile neutrinos in a universe of vacuum energy interacting with cold dark matter *Phys. Dark Univ.* **23** 100261
[129] Knee A M, Contreras D and Scott D 2019 Cosmological constraints on sterile neutrino oscillations from Planck *J. Cosmol. Astropart. Phys.* **2019** 039
[130] Feng L, He D-Z, Li H-L, Zhang J-F and Zhang X 2020 Constraints on active and sterile neutrinos in an interacting dark energy cosmology *Sci. China Phys. Mech. Astron.* **63** 290404
[131] Feng L, Guo R-Y, Zhang J-F and Zhang X 2022 Cosmological search for sterile neutrinos after Planck 2018 *Phys. Lett.* B **827** 136940
[132] Di Valentino E, Gariazzo S, Giunti C, Mena O, Pan S and Yang W 2022 Minimal dark energy: key to sterile neutrino and Hubble constant tensions? *Phys. Rev.* D **105** 103511
[133] Chernikov P A and Ivanchik A V 2022 The influence of the effective number of active and sterile neutrinos on the determination of the values of cosmological parameters *Astron. Lett.* **48** 689–701
[134] Pan S, Seto O, Takahashi T and Toda Y 2023 Constraints on sterile neutrinos and the cosmological tensions *Phys. Rev.* D **110** 083524
[135] Verde L, Treu T and Riess A G 2019 Tensions between the early and the late Universe *Nature Astron.* **3** 891 7
[136] Vitale S, Farr W M, Ng K and Rodriguez C L 2019 Measuring the star formation rate with gravitational waves from binary black holes *Astrophys. J. Lett.* **886** L1
[137] Yang T 2021 Gravitational-wave detector networks: standard sirens on cosmology and modified gravity theory *J. Cosmol. Astropart. Phys.* **05** 044
[138] Belgacem E, Dirian Y, Foffa S, Howell E J, Maggiore M and Regimbau T 2019 Cosmology and dark energy from joint gravitational wave-GRB observations *J. Cosmol. Astropart. Phys.* **2019** 015
[139] Chen Z-C, Huang F and Huang Q-G 2019 Stochastic gravitational-wave background from binary black holes and binary neutron stars and implications for LISA *Astrophys. J.* **871** 97
[140] Du M and Xu L 2022 How will our knowledge of short gamma-ray bursts affect the distance measurement of binary neutron stars? *Sci. China Phys. Mech. Astron.* **65** 219811
[141] de Souza J M S and Sturani R 2021 Cosmological model selection from standard siren detections by third-generation gravitational wave observatories *Phys. Dark Univ.* **32** 100830
[142] Regimbau T, Evans M, Christensen N, Katsavounidis E, Sathyaprakash B and Vitale S 2017 Digging deeper: Observing primordial gravitational waves below the binary black hole produced stochastic background *Phys. Rev. Lett.* **118** 151105
[143] Belgacem E, Dirian Y, Foffa S and Maggiore M 2018 Modified gravitational-wave propagation and standard sirens *Phys. Rev.* D **98** 023510
[144] Safarzadeh M, Berger E, Ng K K Y, Chen H-Y, Vitale S, Whittle C and Scannapieco E 2019 Measuring the delay time distribution of binary neutron stars. II. Using the redshift distribution from third-generation gravitational wave detectors network *Astrophys. J. Lett.* **878** L13
[145] Song H-R, Ai S-K, Wang M-H, Xing N, Gao H and Zhang B 2019 Viewing angle constraints on S190425z and S190426c and the joint gravitational-wave/gamma-ray detection fractions for binary neutron star mergers *Astrophys. J. Lett.* **881** L40
[146] Wanderman D and Piran T 2015 The rate, luminosity function and time delay of non-collapsar short GRBs *Mon. Not. Roy. Astron. Soc.* **448** 3026–37
[147] Yu J, Song H, Ai S, Gao H, Wang F, Wang Y, Lu Y, Fang W and Zhao W 2021 Multimessenger detection rates and distributions of binary neutron star mergers and their cosmological implications *Astrophys. J.* **916** 54
[148] Regimbau T, Siellez K, Meacher D, Gendre B and Boër M 2015 Revisiting coincidence rate between gravitational wave detection and short gamma-ray burst for the advanced and third generation *Astrophys. J.* **799** 69
[149] Madau P and Dickinson M 2014 Cosmic star formation history *Ann. Rev. Astron. Astrophys.* **52** 415–86

[150] Eichhorn A, Koslowski T and Pereira A D 2019 Status of background-independent coarse-graining in tensor models for quantum gravity *Universe* **5** 53
[151] Abbott R *et al* 2023 Population of merging compact binaries inferred using gravitational waves through GWTC-3 *Phys. Rev.* X **13** 011048
[152] Abbott B P *et al* 2019 GWTC-1: A gravitational-wave transient catalog of compact binary mergers observed by LIGO and virgo during the first and second observing runs *Phys. Rev.* X **9** 031040
[153] Özel F and Freire P 2016 Masses, radii, and the equation of state of neutron stars *Ann. Rev. Astron. Astrophys.* **54** 401–40
[154] Zhang X, Liu T and Zhao W 2017 Gravitational radiation from compact binary systems in screened modified gravity *Phys. Rev.* D **95** 104027
[155] Zhao W and Wen L 2018 Localization accuracy of compact binary coalescences detected by the third-generation gravitational-wave detectors and implication for cosmology *Phys. Rev.* D **97** 064031
[156] Wen L and Chen Y 2010 Geometrical expression for the angular resolution of a network of gravitational-wave detectors *Phys. Rev.* D **81** 082001
[157] Curt Cutler *et al* 1993 The last three minutes: issues in gravitational wave measurements of coalescing compact binaries *Phys. Rev. Lett.* **70** 2984–7
[158] Sathyaprakash B S and Schutz B F 2009 Physics, astrophysics and cosmology with gravitational waves *Living Rev. Rel.* **12** 2
[159] Howell E J, Ackley K, Rowlinson A and Coward D 2018 Joint gravitational wave—gamma-ray burst detection rates in the aftermath of GW170817 *Mon. Not. Royal Astron. Soc.* **485** 1435–47
[160] Tan W-W and Yu Y-W 2020 The jet structure and the intrinsic luminosity function of short gamma-ray bursts *Astrophys. J.* **902** 83
[161] Stratta G, Amati L, Ciolfi R and Vinciguerra S 2018 THESEUS in the era of multi-messenger astronomy arXiv:1802.01677
[162] Speri L, Tamanini N, Caldwell R R, Gair J R and Wang B 2021 Testing the quasar Hubble diagram with LISA standard sirens *Phys. Rev.* D **103** 083526
[163] Hirata C M, Holz D E and Cutler C 2010 Reducing the weak lensing noise for the gravitational wave Hubble diagram using the non-Gaussianity of the magnification distribution *Phys. Rev.* D **81** 124046
[164] Kocsis B, Frei Z, Haiman Z and Menou K 2006 Finding the electromagnetic counterparts of cosmological standard sirens *Astrophys. J.* **637** 27–37
[165] Aghanim N *et al* 2020 Planck 2018 results. VI. Cosmological parameters *Astron. Astrophys.* **641** A6
[Erratum: Astron. Astrophys. 652, C4 (2021)] (https://doi.org/10.1051/0004-6361/201833910)
[166] Beutler F, Blake C, Colless M, Jones D H, Lister S-S, Campbell L, Parker Q, Saunders W and Watson F 2011 The 6dF galaxy survey: Baryon acoustic oscillations and the local hubble constant *Mon. Not. Roy. Astron. Soc.* **416** 3017–32
[167] Ross A J, Samushia L, Howlett C, Percival W J, Burden A and Manera M 2015 The clustering of the SDSS DR7 main Galaxy sample - I. A 4 per cent distance measure at $z = 0$: 15 *Mon. Not. Roy. Astron. Soc.* **449** 835–47
[168] Alam S *et al* 2017 The clustering of galaxies in the completed SDSS-III Baryon Oscillation Spectroscopic Survey: cosmological analysis of the DR12 galaxy sample *Mon. Not. Roy. Astron. Soc.* **470** 2617–52
[169] Scolnic D M *et al* 2018 The complete light-curve sample of spectroscopically confirmed SNe Ia from Pan-STARRS1 and cosmological constraints from the combined pantheon sample *Astrophys. J.* **859** 101
[170] Lewis A and Bridle S 2002 Cosmological parameters from CMB and other data: A Monte Carlo approach *Phys. Rev.* D **66** 103511
[171] https://www.et-gw.eu/index.php/etsensitivities/
[172] https://cosmicexplorer.org/sensitivity.html
[173] Zhu J-P *et al* 2023 Kilonovae and optical sfterglows from binary neutron star mergers. II. optimal search strategy for serendipitous observations and target-of-opportunity observations of gravitational wave triggers *Astrophys. J.* **942** 88